Quantitative brain MRI at 7T in healthy subjects and in metabolic diseases

6.

SUMMARY AND GENERAL DISCUSSION

A growing amount of evidence shows that clinical, but also fundamental neuroscientific studies benefit from ultra-high field MRI (Trattnig *et al.*, 2016; Ugurbil, 2017). Because of the higher SNR (Pohmann *et al.*, 2016), 7T MRI is able to provide anatomical and functional images with great detail and contrast, without jeopardizing patient comfort and, hereby, outperforming field strengths that are typically used in the clinic (≤ 3T). As such, the imaging community is pushing ultra-high field MRI forward, which recently led to the CE certificate and FDA approval for the Siemens 7T Magnetom Terra scanner, paving the way for clinical use in Europe and North America, respectively. The number of research centers that operate 7T MRI scanners has steadily increased in the last years and has led to tremendous improvements in hardware, instrumentation and sequence design (Ugurbil, 2017; Polimeni and Uludağ, 2018). Consequentially, it becomes possible to acquire high quality, high resolution, multi-parametric data within an hour. Depending on the specific research aims and/or study population, several choices have to be made for the design of the imaging protocol: (i) weighted or quantitative imaging (not mutually exclusive), (ii) type of contrasts (e.g. T_1, $T_2^{(*)}$, MT, perfusion, diffusion, fMRI), (iii) spatial (and temporal) resolution and (iv) spatial coverage (Marques and Norris, 2017). Throughout the current thesis, we explored the different properties and applications of a multi-parameter, quantitative protocol in healthy subjects and in metabolic diseases. This protocol was developed to capture the biochemical (i.e. microstructure) and metabolic (i.e. blood flow) properties of the brain. In this chapter, we first briefly summarize the work presented in this thesis, followed by a discussion on several related issues and developments that are central to consider for a more broad use of the protocol. Finally, we conclude with a description of a potential application and work in progress not explored in this thesis.

6.1. | SUMMARY

The MP2RAGE sequence is widely used for anatomical imaging at 7T (Marques *et al.*, 2010). Initially developed on the Siemens system platform, it has also been extended towards other 7T vendors (Mougin *et al.*, 2016). In addition to the standard acquisition of a T_1w image, a quantitative T_1 map is obtained in this approach, allowing studying brain microstructure besides morphology. However, B_1^+-related image artifacts – too strong to correct by using dielectric pads (Teeuwisse *et al.*, 2012) and specialized adiabatic inversion pulses (Hurley *et al.*, 2010) – hamper accurate analyses in the affected regions. Especially brain regions that suffer from severe local field inhomogeneity effects, such as the inferior temporal and frontal lobes, are difficult to properly segment into white (WM), gray matter (GM) and cerebrospinal fluid (CSF). As a result, tedious manual corrections of the automatic image segmentations are necessary to

correct for these errors and causes excessive amounts of work, in particular in large-scale imaging studies. Therefore, in **Chapter 2**, we explored the benefits on cortical thickness measurements and T_1(w) contrast when the B_1^+-related variations across the cortex are taken into account using the Sa2RAGE B_1^+ map. By doing so, substantial improvement in the delineation between WM, GM and CSF could be achieved due to the locally improved contrast between tissue types. This resulted in more accurate cortical thickness measurements, shown by the increased correspondence with a normative dataset. In addition, we showed that the cortical T_1 values were significantly biased by the non-uniform RF transmit efficiency prior to the post-hoc B_1^+ correction, leading to artificially increased variation across the cortex. The latter phenomenon was significantly reduced after the correction, revealing the typical myelin-related pattern observed in earlier and lower field strength studies (Glasser and Van Essen, 2011; Lutti *et al.*, 2014). Similar improvements (e.g. increased inter-tissue type contrast) has also been shown for the subcortical GM structures (Marques and Gruetter, 2013). Taken together, these results have important implications for future studies that use the MP2RAGE data for morphological and/or microstructural analyses. Similar biases are also expected for other T_1 acquisition approaches (e.g. also in the standard T_1w images using MPRAGE, the WM/GM contrast is low in the anterior temporal lobe). Finally, supported by its easy implementation and short scanning duration, this correction step should be part of any users' MP2RAGE data pre-processing workflow.

Following up on the work from the previous chapter to obtain more accurate surface reconstructions of the brain, **Chapter 3** compares the performance of several popular myelin-based mapping approaches using anatomical 7T data. Here, reproducibility and reliability of weighted and quantitative T_1 (i.e. corrected for the B_1^+ bias field, explained above), T_2* and their ratio were compared in terms of contrast-to-noise ratio (CNR), parcellation reliability (i.e. 'parcellability'), and inter- and intra-subject variability and reproducibility. Quantitative MRI methods are considered more robust compared to their weighted counterparts in terms of non-biochemical influences, due to their dominant dependence on intrinsic tissue properties, such as longitudinal (T_1) or transversal relaxation times (T_2*). In contrast, weighted imaging is additionally affected by non-biochemical factors, such as sensitivity to MRI acquisition parameters and image imperfections (e.g. B_0 and B_1 inhomogeneities). As such, quantitative MRI allows more reliable and biology-relevant comparisons within subjects and between healthy subjects and patients. However, while both types of contrasts (i.e. quantitative vs. weighted) may be appropriate to accurately capture the variation of myelin and iron concentration across the cortex within a subject (but not necessarily across subjects), they were previously not systematically compared at 7T. In our study, similar but not

identical myelination patterns were observed across all tested contrasts. However, we found that CNR per unit time and parcellability were lower for the transversal compared to the longitudinal relaxation parameters. In addition, quantitative R_1 (=1/T_1) turned out to be the most reliable parameter to map the myelin distribution compared to the other parameters. The respective maps were characterized by the lowest inter- and intra-subject coefficient of variation. In addition, these spatial surface maps can be used for microstructure-informed delineation of cortical areas. We explored two area-defining methods: (i) thresholding the MR parameter values and (ii) surface gradients of these values, to determine areal borders based on the cortical surface pattern. Both methods are partially observer-dependent, needing manual interaction (i.e., choice of threshold or connecting high gradient values) to provide unambiguous borders. In order to obtain fully data-driven cortical parcellations and to overcome this observer-dependency, several methods have been developed in this emerging field. We will briefly discuss this topic later in this chapter and show some examples.

Similar to the studies presented in Chapters 2 and 3, we acquired quantitative MRI data, additionally including cerebral blood flow (CBF), in metabolic diseases. Here, the MRI data were combined with genetic analyses in order to relate morphological-, microstructural- and metabolic-related variations in the brain, measured using MRI, to genetic differences across the study population (i.e. 'imaging genetics'). This was performed in a metabolic disease, for which the genetic underpinning is well established and only the mutation load varies between patients (Chapter 4) and in Type 2 Diabetes Mellitus (T2DM), a more complex polygenetic disorder (Chapter 5). In **Chapter 4**, we examined patients with m.3243A>G mutation; this mutation affects the mitochondrial DNA and leads to the expression of a widely varying phenotype across the patient population. Symptoms often observed include hearing loss, development of (mitochondrial) diabetes, muscle atrophy, as well as tissue changes in the brain. Interestingly, the number of mutated mitochondria in a single cell, referred to as 'mutation load', differs across tissue types (i.e. blood and urine epithelial cells), but also between patients. Previous studies have shown that the disease severity positively correlates with the mutation load measured across several tissue types. However, none of them investigated potential brain correlates. Therefore, the aim of the small-scale imaging genetics study was to assess to this relation using the mutation load in blood and urine. In our patient population, the mutation loads in blood and urine significantly correlated with disease severity, confirming the observations in earlier studies. We found a strong correlation between brain volume and both mutation loads, however, more strongly for that measured in blood. Cortical GM, WM and cerebellar GM volume significantly decreased with increasing mutation load. Interestingly, subcortical GM

(i.e. putamen and globus pallidus) volume was lower for the m.3243A>G patients compared to controls, but no mutation load effect was observed. In addition, clusters of vertices were identified, where cortical thickness significantly decreased, while T_1, T_2* and CBF tend to increase as function of mutation load. These clusters spanned specific areas involved in auditory processing (e.g. auditory cortex) and those that are characterized by a higher resting-state connectivity (e.g. default-mode and default-attention networks). These observations can be linked to the clinical symptoms in m.3243A>G patients, such as hearing loss and decreased attentional/executive functioning. These results may guide future MRI, but also in vitro, studies to track disease pathogenesis and relationship with specific clinical symptoms.

While the work and analyses in Chapter 4 are straightforward, the population and analysis strategies presented in **Chapter 5** are more challenging. In this chapter, the main focus was to highlight the different types of data and discuss potential analyses strategies, in addition to providing a brief description of the preliminary output from the proposed analyses workflows. The clinical characteristics of the study population confirmed the significant differences in the cardiovascular profiles (e.g. blood glucose and lipid levels) across groups, which was expected based on the group-specific inclusion criteria. Ultimately, the data will be analyzed from different perspectives with the aim to develop multi-level biomarkers in metabolic syndrome (MetS) and T2DM. Due to the complex genetic nature of T2DM, the high dimensionality of the data, and the possibility to merge multiple data modalities (i.e. MRI, genetic, metabolomic, cognitive and clinical), more advanced statistical methods have to be utilized to identify T2DM biomarkers. For this, the availability of each dataset can be used to good advantage. For example, we showed a cluster of metabolites that were present in distinct quantities in T2DM subjects compared to controls. Therefore, characterization of the related metabolic pathways, based on this data, may provide clues for narrowing down analyses, and formulation of specific hypotheses with regards to the whole-exome sequencing data.

While interesting from an imaging genetics or 'imaging -omics' point of view, the presented dataset also provides opportunities to explore each data modality separately. Genotype-phenotype relationships, as well as metabolomic profiles, can be established to define modality-specific biomarkers that potentially might aid the explanation of phenotypical and functional differences across subjects/groups. However, the sample size (N=133) – even though high for a 7T study – is rather limited for genetic and metabolomic studies, for which sample sizes of >1000 are preferred. Dimensionality reduction/feature selection (i.e. filtering) techniques, such as independent

component analysis, but also methods using prior knowledge (Kircher *et al.*, 2014), become more important (Saeys *et al.*, 2007). This is less crucial for the MRI part, as it represents a rich and unique dataset that can be used to answer several modality-specific research questions. For example, the submillimeter resolution of the anatomical data provides spatial details that can be used to identify small-scale structural changes in the brain as a result of impaired glucose metabolism. This includes changes in tissue susceptibility due to cerebral microbleeds or iron depositions. Also more methodologically relevant questions can be answered, such as the relationship between blood T_1 and hematocrit levels and how this changes in T2DM, an issue important for the quantification of cerebral blood flow using ASL (Xu *et al.*, 2018). Across all applications of 7T MRI described in this thesis, it is important to monitor and evaluate data quality, crucial for implementing these approaches in clinical populations. Therefore, in the following, we will address some of the issues encountered for the different imaging contrasts and describe potential technological developments that may be able to overcome these.

6.2. | STANDARDIZATION AND HARMONIZATION OF CLINICAL QUANTITATIVE 7T MRI

It has been highlighted throughout this thesis that 7T imaging provides a number of advantages compared to lower field strengths. In addition, the presented data demonstrates the possibility to acquire whole-brain high resolution anatomical, perfusion and functional data within an hour and its application to study neurodegeneration in a clinical population. However, the potential of 7T reaches far beyond what is demonstrated in this thesis, including fMRI (Uludag and Blinder, 2017), spectroscopy (Bogner *et al.*, 2011), diffusion (Vu *et al.*, 2015) and vascular imaging (De Cocker *et al.*, 2016). The addition of such measurements will complement our protocol and boosts the range of applications it can be used for. Quality assessment, standardization and harmonization of MRI protocols are essential in order to allow utilization and generalization of such protocols across studies, imaging sites and scanner vendors.

Acquisition of large-scale datasets, too expensive to cover by individual institutions, as well as those in rare diseases, such as in m.3243A>G patients, can be promoted due to the possibilities to pool data across multiple imaging sites. Several nation-wide and international 7T networks have been established to serve this purpose, such as the German Ultra High Field Imaging (GUFI) and United Kingdom's 7T (UK7T) networks and European Ultra-high field Imaging Network for Neurodegenerative Diseases (EUFIND). These consortia aim to set up standardized sequences across the main 7T suppliers that limit the effect of hard- (e.g. coils and gradients) and software (e.g. imaging

sequence implementations and reconstruction methods) differences. Sequences and corresponding parameters need to be chosen in such a way that they are applicable across Siemens, Philips and General Electric (GE) systems and provide comparable data in terms of temporal and spatial SNR and CNR. Here, it is important to find the right balance between conformity across vendors and maximal performances within vendor (i.e. not necessarily accepting a 'least common denominator' solution). The generalizability of clinical MRI depends on the comparability of the data generated at different sites, scanner vendors and time points (Voelker *et al.*, 2016). Quantitative MRI (ideally) overcomes potential, non-biochemical inter-site, intra-subject biases that are present in weighted MRI data, which hinder the direct comparison across studies and between patients and healthy controls. Hereafter, we will address some of the quality-related issues that were encountered while acquiring and analyzing the presented data.

6.2.1. | *Anatomical imaging*

The results in Chapters 2 and 3 demonstrated that the quality of anatomical data acquired at 7T depends on the type of contrast. Here, quantitative T_1 maps were more robust across subjects and within subjects, compared to their weighted counterparts. However, in order to obtain more precise T_1 maps, we show that homogeneous RF transmit profiles are important, even for quantitative data. To limit possible confounding effects due to this, sequence (i.e. MP2RAGE, in this case) parameters can be optimized in such a way that the B_1^+ dependency is decreased or, alternatively, CNR is increased, depending on the specific study aim (Marques and Gruetter, 2013). In contrast, quantitative T_2* maps were characterized by a much higher variation and sensitivity for non-biochemical variation, in line with previous findings at lower field strengths (Weiskopf *et al.*, 2013). This lower reproducibility can be partly ascribed to susceptibility artifacts near the inferior temporal and frontal regions. Although lower in high resolution data, due to smaller intra-voxel spin phase coherence loss, also SNR differences across echo times may lead to noise enhancement when fitting the T_2*-weighted data. Inclusion of more echo times, and potentially, a longer maximal echo time may improve the precision of the T_2* maps, at the cost of prolonging acquisition times (Cohen-Adad, 2014; Govindarajan *et al.*, 2015). This would additionally enable the use of more advanced (i.e. mono-exponential vs. multi-exponential) fitting models to gain quantification accuracy and biochemical specificity (van Gelderen *et al.*, 2012). Alternatively, T_2 (i.e. transversal relaxation time for spin-echo sequences, less affected by local field inhomogeneities), instead of T_2*, imaging, may yield more reproducible data. However, as for now, acquisition of whole-brain T_2-weighted images at 7T remains challenging due to inhomogeneous transmit profiles, power deposition

limitations and long acquisition times using conventional single-channel transmission. In addition, T_2* maps may be more biochemically informative, due to its higher dependency on local changes in iron concentration (Cohen-Adad, 2014; Stuber *et al.*, 2014).

6.2.2. | Perfusion imaging

While anatomical and functional imaging at 7T benefit from ultra-high field strengths, this is less evident for ASL imaging. Compared to the T_1 and T_2* maps, ASL data presumably harbors lower SNR and CNR. Although improvements were observed compared to lower fields strengths, in particular at higher spatial resolutions (Gardener *et al.*, 2009; Ivanov *et al.*, 2017), ASL suffers from persisting problems (Teeuwisse *et al.*, 2010). The upper limit of ASL SNR is determined by the low GM microvascular density (~1%–2% of local tissue volume) and signal reduction due to T_1 recovery after labeling. Especially for clinical purposes, when scanning time is a limiting factor, increasing the SNR is challenging. In addition, acquisition of whole-brain CBF maps remains an issue, as well as the sensitivity of CBF acquisitions to subject motion. Several possible practical solutions have been explored to maximize data quality. These include, for example, the use of dielectric pads, and optimized positioning of the head and magnet isocenter reference to improve to B_1^+ homogeneity and labeling efficiency, respectively (Ghariq *et al.*, 2012). Also, several improvements in sequence design have been proposed to increase coverage without increasing scan time. This includes the implementation of echo-planar imaging (EPI) readouts, parallel (e.g. generalized autocalibrating partially parallel acquisitions, GRAPPA), simultaneous multi-slice (SMS, which also reduces motion sensitivity) or multi-band (MB) imaging (Feinberg *et al.*, 2013; Kim *et al.*, 2013; Ivanov *et al.*, 2017). While these methods may lead to losses in (temporal) SNR, the sequence parameters in the current protocol were chosen such that the loss in (t)SNR was kept minimal for maximal brain coverage (~80%) (see also Ivanov *et al.* (2017) and references herein for more details and an in-depth discussion of ASL at UHF). To conclude, ASL is a promising tool to measure brain perfusion non-invasively; however, future studies and technical developments (see below) are necessary to reach its full potential at UHF.

6.3. | TECHNICAL DEVELOPMENTS TO IMPROVE CLINICAL APPLICABILITY OF 7T

Several technical developments are currently being explored to improve the clinical applicability of 7T imaging and to overcome (some of) the limitations described above. This includes, for example, prospective motion correction. Prospective motion correc-

tion can be used for real-time updating of most pulse sequences to reduce artifacts caused by head motion and therefore it has potential to make a large impact in clinical routine (Maclaren *et al.*, 2013). In addition, magnetic field monitoring, to compensate for spatiotemporal field perturbations, is another promising technique to reduce image artifacts and distortion (Barmet *et al.*, 2008). Field control improved the fidelity of T_2* maps by mitigating field changes related to the subject's breathing pattern, for example (Wyss *et al.*, 2017).

The introduction of the parallel (i.e. multi-channel) transmission (pTx) technology has been one of the main developments for UHF imaging. It may resolve some, if not many, of the issues discussed above, by improving the temporal resolution and energy efficiency of the radio-frequency (RF) pulses (Katscher *et al.*, 2003; Zhu, 2004). Advanced coil designs (Shajan *et al.*, 2014; Sengupta *et al.*, 2016) and RF pulses (Setsompop *et al.*, 2008; Poser *et al.*, 2014) are being developed to take full advantage of the technology. Shorter excitations can be achieved without risking data quality reduction, which is particularly beneficial for clinical purposes. Alternatively, it can be used to reduce B_1^+ inhomogeneities and resulting image contrast biases across and within subjects (such as observed in Chapters 2 and 3) and imaging sites, without increasing scan duration (Cloos *et al.*, 2012). In addition, ASL techniques will benefit from parallel transmission by enabling a more tailored labeling field maximizing labeling efficiency (Oliver-Taylor *et al.*, 2012). So far, the majority of current pTx-related studies depended mostly on custom hard- (e.g. coils) and software (e.g. sequences) not publicly available and only little work has been transferred into clinical practice, although clinical applications of dual-transmit systems have been discussed (Brink *et al.*, 2015). Future work is necessary to further assess the advantages of pTx and improve its workflow for clinical routine, for example, by limiting the required user interaction and computational complexity.

6.4. | CLINICAL INTERPRETATION OF QUANTITATIVE 7T MRI

Given the increased spatial resolution and contrast that can be obtained using (quantitative) 7T MRI, better understanding of the biophysical mechanisms and their relation to pathologies, are necessary to improve clinical decision-making. This requires interdisciplinary research to link, for example, changes in tissue composition (e.g. studied by biologists and chemists), due to disease (e.g. pathologists), to differences of the measured MRI signal (e.g. physicists) and specialized data analysis methods (i.e. data scientists), eventually. As such, optimization of quantitative MRI – based on a single or multiple MR parameter(s) – is vital to better reflect the underlying tissue properties and dynamics of biological processes, including changes in the homeostasis of mac-

romolecular compounds due to disease. Here, because of their clinical relevance in, for example, Parkinson's (PD) and Alzheimer's Disease (AD), iron and neuromelanin, have been one of the main targets of such interdisciplinary research (Keren *et al.*, 2015; Bulk *et al.*, 2018). As a result of histological and biochemical validation studies, MRI sequences can be optimized to better image and characterize brain structures in vivo, due to an improved understanding of their biochemical composition (Priovoulos *et al.*, 2017; Ropele and Langkammer, 2017). Obviously, these methods can also be extended towards other clinical phenotypes, including optimized detection of microbleeds and iron depositions in T2DM subjects. Finally, machine-learning methods that target these features, may facilitate diagnosis and prognosis by a clinician.

6.5. | MULTI-PARAMETER, QUANTITATIVE MRI-BASED CORTICAL PARCELLATION

Despite the many advantages of acquiring high-resolution data, continuous developments and prospects for clinical use, its high dimensionality and resulting low statistical power (especially in whole-brain studies), necessitates the improvement of data analysis methods as well. As discussed in Chapter 5, the brain phenotype dimensionality can be reduced using parcellation techniques. By this means, data complexity is decreased while statistical power is increased. Automatic segmentation software packages, such as FreeSurfer, typically use macro-anatomical (gyral and sulcal) landmarks and/or predefined atlases to subdivide the (sub-)cortical GM into distinct regions (Fischl *et al.*, 2004; Desikan *et al.*, 2006). More and more, the focus of MRI-data based cortical parcellation is shifting towards individualized methods based on in vivo morphological (i.e. cortical thickness), microstructural (i.e. T_1 and T_2*) or anatomical (i.e. DTI) and functional (i.e. task- or rs-fMRI) connectivity derivates (Geyer *et al.*, 2011; Yeo *et al.*, 2011; Ganepola *et al.*, 2017).

One of the most important advances in this field was the release of a cortical parcellation map based on multiple modalities, including cortical thickness, myelin content (i.e. T_1/T_2 ratio) and (task- and resting state-based) functional 3T data from the Human Connectome Project (Glasser *et al.*, 2016). Here, a gradient-based parcellation approach was applied to identify areal borders using predefined criteria. These criteria were (i) consistency across modalities, (ii) left-right symmetry, (iii) imaging artifacts independency, (iv) strong statistical differences of modalities across opposite sides of the border and (v) correspondence with published boundary. After identification of the areas on the group-level, machine-learning algorithms were applied to automatically classify/label each region based on the multi-modal fingerprint on an individual basis

in a separate dataset. While the classifier nicely replicated the cortical parcellation across datasets, demonstrating its robustness, it was derived from partially manual procedure used by two neuroanatomists to cross-check and eventually to modify automatically determined areal borders.

In Chapter 3, we applied the same method (i.e. computation of gradients) on the T_1 and T_2* surface maps. Small differences, for example close to the auditory cortex, were noticeable between T_1 and T_2*-based boundaries across the cortex. This confirms that the T_1 and T_2* contrasts are not redundant and provide complimentary information. However, the borders varied in quality depending on the parameter and were not continuous, therefore demanding observer input when comparing parameters (i.e., a choice of the gradient threshold value and filling-in gaps in the borders). As such, other studies have explored ways to obtain fully-automatic, data-driven cortical parcellations, based on, for example, clustering techniques. Methods to perform such operations at the single-subject or group-based level, using a single modality (i.e. fMRI) instead, have been recently systematically compared (Arslan *et al.*, 2017). They show that, from the tested methods, none of them outperformed the others. Prioritization of the evaluated method characteristics (e.g. reproducibility, cluster validity or other) may guide the method of choice. In addition, other factors to consider are the: (i) single-subject and group-based performance and possibility to include (ii) multiple contrasts and (iii) spatial constraints.

While none of the previous studies in the field of cortical parcellation explored the use of CBF, the 7T data presented in this thesis provides excellent opportunities to explore the benefits of including additional information based on the brain's baseline perfusion (i.e. CBF). Since CBF is closely coupled to brain metabolism (Raichle, 1998), a data-driven parcellation of brain regions that incorporates perfusion information will presumably enhance subsequent functional analysis. Previous studies demonstrated that perfusion could be used to differentiate primary from secondary auditory and visual areas due to a higher vascular density and metabolic demands (Weber *et al.*, 2008; Gardumi *et al.*, 2017). Preliminary analyses using current data showed that the effect of CBF inclusion is different across sets of regions, presumably related to the differences in baseline brain metabolism across the brain (Haast *et al.*, 2017). The CBF data exhibited a spatial pattern different from T_1, T_2* and cortical thickness, e.g. similar higher perfusion can be clearly observed in the occipital lobe and posterior cingulate cortex, while T_1 displays differences between these two areas. It should be noted, however, that the CBF data were acquired with a lower spatial resolution, and therefore, has lower spatial specificity. As these results are promising, we are currently

extending this towards a fully automatic single-subject and/or group-based cortical parcellation routine, using hierarchical clustering that is driven by multiple parameters.

Hierarchical clustering aims to identify voxels or vertices with comparable characteristics based on single or multiple contrasts (Thirion *et al.*, 2014). In addition, spatial constraints can be imposed on the clustering, leading to clusters containing connected voxels or vertices only. As such, clusters are only formed from parents that share neighboring voxels/vertices based on a predefined connectivity matrix. Fig. 6.1 shows an example group-average (N=15) cortical parcellation ($N_{regions}$=180) based on surface maps computed from the quantitative T_1, T_2*, CBF and cortical thickness data presented in Chapter 4 (control subjects). We used the spatially-constrained Ward's hierarchical clustering algorithm implemented in the SciKit-learn toolbox (Ward Jr, 1963; Pedregosa *et al.*, 2011). In particular, Ward's algorithm is very efficient in processing high-dimensional MRI data. This preliminary multi-parameter cortical parcellation, for example, divides the cingulate cortex into separate regions and also reveals the typically shape of the motor cortex.

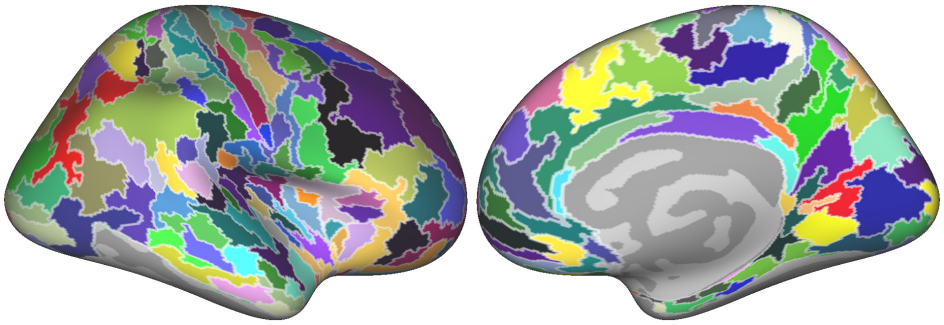

Fig. 6.1. | Multi-parameter cortical parcellation. Quantitative cortical thickness, T1, T2 and CBF data from 15 subjects were used to parcellate the cortical GM into separate regions ($N_{regions}$=180). Please note that the inferior temporal gyrus is masked out as it suffers from strong susceptibility-related artifacts.*

However, in contrast to the gradients-based method, hierarchical clustering requires the number of clusters to be pre-defined. In the example above, we selected the same number of regions found in the paper by Glasser *et al.* (2016). Several methods can be used to find the optimal number of clusters based on the available data. This includes, for example, the Silhouette index, which scores the (data-wise) closeness of each vertex in one cluster to vertices in the neighboring clusters (Rousseeuw, 1987). In addition, bootstrap metrices to evaluate clustering consistency (e.g. adjusted mutual index or adjusted rand index) or cross-validation procedures may be appropriate to find the optimal number of clusters or test the effect of CBF on the cortical parcel-

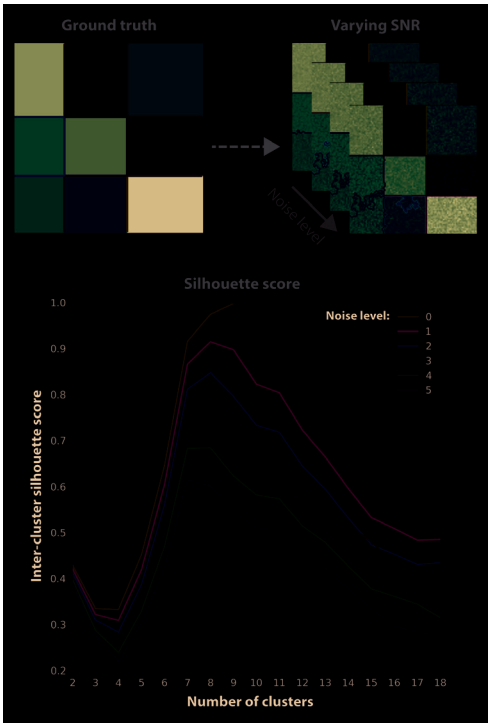

Fig. 6.2. | Evaluation of the Silhouette score for finding the optimal number of clusters using simulated data with varying levels of noise. As can be observed and as expected, the performance of the Silhouette score (i.e. 1 suggests optimal delineation between areas) decreases with increasing noise levels.

lation (Thirion *et al.*, 2014). However, the problem of number of parcels optimization remains open and should be addressed in a data-driven fashion, including simulations. We are currently characterizing, using simulations, the behavior of several methods that aim at identifying the optimal number of clusters. Here, we generate spatial 2D patterns, representing a single parameter, with a known ground truth (i.e. number of clusters) and varying levels of noise. This can be extended to multi-parametric data with corresponding levels of noise (i.e. mimicking the intensity range and quality of cortical thickness, T_1, T_2* and CBF maps) and to patterns more closely resembling the brain's structure. For example, Fig. 6.2 shows the Silhouette scores for clustering performance across a range of $N_{clusters}$ (i.e. 1 suggests optimal cluster separation), based on simulated single parameter data with varying noise and a known ground truth ($N_{clusters}$ = 9). Here, the same clustering method was used as for the example in Fig. 6.1, using Ward's criteria and connectivity constraints and shows that performance of the Silhouette score decreases with increasing noise levels. Finally, extending this work towards the larger dataset described in Chapter 5 can address its reproducibility/stability across multiple datasets, as well as identify regions that are most distinct between controls and T2DM or correlate with specific cognitive scores, which are expected to be found mostly in the frontal and temporal lobe.

6.6. | CONCLUSION

Taken together, the work in this thesis demonstrated possible applications of a standard quantitative brain 7T MRI protocol. The possibilities of 7T MRI are far-reaching and need continuous developments, ranging from development of hardware to

analysis software, that enable acquisition of high quality data and processing this data in the most optimal way. The current work extends earlier studies that have shown that 7T MRI is feasible and superior in many instances to 3T MRI and that we are at the doorstep of its routine use in both healthy subjects and diverse clinical populations, eventually combined with other data modalities.

6.7. | REFERENCES

Arslan, S., S. I. Ktena, A. Makropoulos, E. C. Robinson, D. Rueckert and S. Parisot (2017). "Human brain mapping: A systematic comparison of parcellation methods for the human cerebral cortex." Neuroimage.

Barmet, C., N. De Zanche and K. P. Pruessmann (2008). "Spatiotemporal magnetic field monitoring for MR." Magn Reson Med 60(1): 187-197.

Bogner, W., M. Chmelik, O. C. Andronesi, A. G. Sorensen, S. Trattnig and S. Gruber (2011). "In vivo 31P spectroscopy by fully adiabatic extended image selected in vivo spectroscopy: a comparison between 3 T and 7 T." Magn Reson Med 66(4): 923-930.

Brink, W. M., V. Gulani and A. G. Webb (2015). "Clinical applications of dual-channel transmit MRI: A review." J Magn Reson Imaging 42(4): 855-869.

Bulk, M., W. M. Abdelmoula, R. J. A. Nabuurs, L. M. van der Graaf, C. W. H. Mulders, A. A. Mulder, . . . L. van der Weerd (2018). "Postmortem MRI and histology demonstrate differential iron accumulation and cortical myelin organization in early- and late-onset Alzheimer's disease." Neurobiol Aging 62: 231-242.

Cloos, M., N. Boulant, M. Luong, G. Ferrand, E. Giacomini, D. Le Bihan and A. Amadon (2012). "kT-points: short three-dimensional tailored RF pulses for flip-angle homogenization over an extended volume." Magnetic resonance in medicine 67(1): 72-80.

Cohen-Adad, J. (2014). "What can we learn from T2* maps of the cortex?" Neuroimage 93 Pt 2: 189-200.

De Cocker, L. J., A. Lindenholz, J. J. Zwanenburg, A. G. van der Kolk, M. Zwartbol, P. R. Luijten and J. Hendrikse (2016). "Clinical vascular imaging in the brain at 7T." Neuroimage.

Desikan, R. S., F. Segonne, B. Fischl, B. T. Quinn, B. C. Dickerson, D. Blacker, . . . R. J. Killiany (2006). "An automated labeling system for subdividing the human cerebral cortex on MRI scans into gyral based regions of interest." Neuroimage 31(3): 968-980.

Feinberg, D. A., A. Beckett and L. Chen (2013). "Arterial spin labeling with simultaneous multislice echo planar imaging." Magn Reson Med 70(6): 1500-1506.

Fischl, B., A. van der Kouwe, C. Destrieux, E. Halgren, F. Segonne, D. H. Salat, . . . A. M. Dale (2004). "Automatically parcellating the human cerebral cortex." Cereb Cortex 14(1): 11-22.

Ganepola, T., Z. Nagy, A. Ghosh, T. Papadopoulo, D. C. Alexander and M. I. Sereno (2017). "Using diffusion MRI to discriminate areas of cortical grey matter." Neuroimage.

Gardener, A. G., P. A. Gowland and S. T. Francis (2009). "Implementation of quantitative perfusion imaging using pulsed arterial spin labeling at ultra-high field." Magn Reson Med 61(4): 874-882.

Gardumi, A., D. Ivanov, M. Havlicek, E. Formisano and K. Uludag (2017). "Tonotopic maps in human auditory cortex using arterial spin labeling." Hum Brain Mapp 38(3): 1140-1154.

Geyer, S., M. Weiss, K. Reimann, G. Lohmann and R. Turner (2011). "Microstructural Parcellation of the Human Cerebral Cortex - From Brodmann's Post-Mortem Map to in vivo Mapping with High-Field Magnetic Resonance Imaging." Front Hum Neurosci 5: 19.

Ghariq, E., W. M. Teeuwisse, A. G. Webb and M. J. van Osch (2012). "Feasibility of pseudocontinuous arterial spin labeling at 7 T with whole-brain coverage." MAGMA 25(2): 83-93.

Glasser, M. F., T. S. Coalson, E. C. Robinson, C. D. Hacker, J. Harwell, E. Yacoub, . . . D. C. Van Essen (2016). "A multi-modal parcellation of human cerebral cortex." Nature 536(7615): 171-178.

Glasser, M. F. and D. C. Van Essen (2011). "Mapping human cortical areas in vivo based on myelin content as revealed by T1- and T2-weighted MRI." J Neurosci 31(32): 11597-11616.

Govindarajan, S. T., J. Cohen-Adad, M. P. Sormani, A. P. Fan, C. Louapre and C. Mainero (2015). "Reproducibility of T2 * mapping in the human cerebral cortex in vivo at 7 tesla MRI." J Magn Reson Imaging 42(2): 290-296.

Haast, R. A., D. Ivanov, E. Formisano and K. Uludag (2017). "Cerebral blood flow as a marker for cortical parcellation." Proc. Intl. Soc. Mag. Reson. Med. 25: 352.

Hurley, A. C., A. Al-Radaideh, L. Bai, U. Aickelin, R. Coxon, P. Glover and P. A. Gowland (2010). "Tailored RF pulse for magnetization inversion at ultrahigh field." Magn Reson Med 63(1): 51-58.

Ivanov, D., A. Gardumi, R. A. M. Haast, J. Pfeuffer, B. A. Poser and K. Uludag (2017). "Comparison of 3T and 7T ASL techniques for concurrent functional perfusion and BOLD studies." Neuroimage 156: 363-376.

Ivanov, D., B. A. Poser, L. Huber, J. Pfeuffer and K. Uludag (2017). "Optimization of simultaneous multislice EPI for concurrent functional perfusion and BOLD signal measurements at 7T." Magn Reson Med 78(1): 121-129.

Katscher, U., P. Börnert, C. Leussler and J. S. Van Den Brink (2003). "Transmit sense." Magnetic resonance in medicine 49(1): 144-150.

Keren, N. I., S. Taheri, E. M. Vazey, P. S. Morgan, A. C. Granholm, G. S. Aston-Jones and M. A. Eckert (2015). "Histologic validation of locus coeruleus MRI contrast in post-mortem tissue." Neuroimage 113: 235-245.

Kim, T., W. Shin, T. Zhao, E. B. Beall, M. J. Lowe and K. T. Bae (2013). "Whole brain perfusion measurements using arterial spin labeling with multiband acquisition." Magn Reson Med 70(6): 1653-1661.

Kircher, M., D. M. Witten, P. Jain, B. J. O'Roak, G. M. Cooper and J. Shendure (2014). "A general framework for estimating the relative pathogenicity of human genetic variants." Nat Genet 46(3): 310-315.

Lutti, A., F. Dick, M. I. Sereno and N. Weiskopf (2014). "Using high-resolution quantitative mapping of R1 as an index of cortical myelination." Neuroimage 93 Pt 2: 176-188.

Maclaren, J., M. Herbst, O. Speck and M. Zaitsev (2013). "Prospective motion correction in brain imaging: a review." Magn Reson Med 69(3): 621-636.

Marques, J. P. and R. Gruetter (2013). "New developments and applications of the MP2RAGE sequence--focusing the contrast and high spatial resolution R1 mapping." PLoS One 8(7): e69294.

Marques, J. P., T. Kober, G. Krueger, W. van der Zwaag, P. F. Van de Moortele and R. Gruetter (2010). "MP2RAGE, a self bias-field corrected sequence for improved segmentation and T1-mapping at high field." Neuroimage 49(2): 1271-1281.

Marques, J. P. and D. G. Norris (2017). "How to choose the right MR sequence for your research question at 7T and above?" Neuroimage.

Mougin, O., R. Abdel-Fahim, R. Dineen, A. Pitiot, N. Evangelou and P. Gowland (2016). "Imaging gray matter with concomitant null point imaging from the phase sensitive inversion recovery sequence." Magn Reson Med 76(5): 1512-1516.

Oliver-Taylor, A., R. Ordidge, C. Randell and D. L. Thomas (2012). "Parallel Transmit Vessel Selective Arterial Spin Labelling: Phantom and In-Vivo Results." Proc. Intl. Soc. Mag. Reson. Med. 20: 1995.

Pedregosa, F., G. Varoquaux, A. Gramfort, V. Michel, B. Thirion, O. Grisel, . . . V. Dubourg (2011). "Scikit-learn: Machine learning in Python." Journal of machine learning research 12(Oct): 2825-2830.

Pohmann, R., O. Speck and K. Scheffler (2016). "Signal-to-noise ratio and MR tissue parameters in human brain imaging at 3, 7, and 9.4 tesla using current receive coil arrays." Magn Reson Med

75(2): 801-809.

Polimeni, J. R. and K. Uludağ (2018). "Neuroimaging with Ultra-High Field MRI: Present and Future." NeuroImage.

Poser, B. A., R. J. Anderson, B. Guérin, K. Setsompop, W. Deng, A. Mareyam, . . . V. A. Stenger (2014). "Simultaneous multislice excitation by parallel transmission." Magnetic resonance in medicine 71(4): 1416-1427.

Priovoulos, N., H. I. L. Jacobs, D. Ivanov, K. Uludag, F. R. J. Verhey and B. A. Poser (2017). "High-resolution in vivo imaging of human locus coeruleus by magnetization transfer MRI at 3T and 7T." Neuroimage.

Raichle, M. E. (1998). "Behind the scenes of functional brain imaging: a historical and physiological perspective." Proc Natl Acad Sci U S A 95(3): 765-772.

Ropele, S. and C. Langkammer (2017). "Iron quantification with susceptibility." NMR Biomed 30(4).

Rousseeuw, P. J. (1987). "Silhouettes: a graphical aid to the interpretation and validation of cluster analysis." Journal of computational and applied mathematics 20: 53-65.

Saeys, Y., I. Inza and P. Larranaga (2007). "A review of feature selection techniques in bioinformatics." Bioinformatics 23(19): 2507-2517.

Sengupta, S., A. Roebroeck, V. G. Kemper, B. A. Poser, J. Zimmermann, R. Goebel and G. Adriany (2016). "A specialized multi-transmit head coil for high resolution fMRI of the human visual cortex at 7T." PloS one 11(12): e0165418.

Setsompop, K., V. Alagappan, B. Gagoski, T. Witzel, J. Polimeni, A. Potthast, . . . L. L. Wald (2008). "Slice-selective RF pulses for in vivo B 1+ inhomogeneity mitigation at 7 tesla using parallel RF excitation with a 16-element coil." Magnetic resonance in medicine 60(6): 1422-1432.

Shajan, G., M. Kozlov, J. Hoffmann, R. Turner, K. Scheffler and R. Pohmann (2014). "A 16-channel dual-row transmit array in combination with a 31-element receive array for human brain imaging at 9.4 T." Magnetic resonance in medicine 71(2): 870-879.

Stuber, C., M. Morawski, A. Schafer, C. Labadie, M. Wahnert, C. Leuze, . . . R. Turner (2014). "Myelin and iron concentration in the human brain: a quantitative study of MRI contrast." Neuroimage 93 Pt 1: 95-106.

Teeuwisse, W. M., W. M. Brink and A. G. Webb (2012). "Quantitative assessment of the effects of high-permittivity pads in 7 Tesla MRI of the brain." Magn Reson Med 67(5): 1285-1293.

Teeuwisse, W. M., A. G. Webb and M. J. van Osch (2010). "Arterial spin labeling at ultra-high field: All that glitters is not gold." International Journal of Imaging Systems and Technology 20(1): 62-70.

Thirion, B., G. Varoquaux, E. Dohmatob and J. B. Poline (2014). "Which fMRI clustering gives good brain parcellations?" Front Neurosci 8: 167.

Trattnig, S., E. Springer, W. Bogner, G. Hangel, B. Strasser, B. Dymerska, . . . S. D. Robinson (2016). "Key clinical benefits of neuroimaging at 7T." Neuroimage.

Ugurbil, K. (2017). "Imaging at ultrahigh magnetic fields: History, challenges, and solutions." Neuroimage.

Uludag, K. and P. Blinder (2017). "Linking brain vascular physiology to hemodynamic response in ultra-high field MRI." Neuroimage.

van Gelderen, P., J. A. de Zwart, J. Lee, P. Sati, D. S. Reich and J. H. Duyn (2012). "Nonexponential T(2) decay in white matter." Magn Reson Med 67(1): 110-117.

Voelker, M. N., O. Kraff, D. Brenner, A. Wollrab, O. Weinberger, M. C. Berger, . . . O. Speck (2016). "The traveling heads: multicenter brain imaging at 7 Tesla." MAGMA 29(3): 399-415.

Vu, A. T., E. Auerbach, C. Lenglet, S. Moeller, S. N. Sotiropoulos, S. Jbabdi, . . . K. Ugurbil (2015). "High resolution whole brain diffusion imaging at 7T for the Human Connectome Project." Neuroimage 122: 318-331.

Ward Jr, J. H. (1963). "Hierarchical grouping to optimize an objective function." Journal of the American statistical association 58(301): 236-244.

Weber, B., A. L. Keller, J. Reichold and N. K. Logothetis (2008). "The microvascular system of the striate and extrastriate visual cortex of the macaque." Cereb Cortex 18(10): 2318-2330.

Weiskopf, N., J. Suckling, G. Williams, M. M. Correia, B. Inkster, R. Tait, . . . A. Lutti (2013). "Quantitative multi-parameter mapping of R1, PD(*), MT, and R2(*) at 3T: a multi-center validation." Front Neurosci 7: 95.

Wyss, M., Y. Duerst, D. Nanz, L. Kasper, B. J. Wilm, B. E. Dietrich, . . . K. P. Pruessmann (2017). "Feedback field control improves the precision of T2 * quantification at 7 T." NMR Biomed 30(10).

Xu, F., W. Li, P. Liu, J. Hua, J. J. Strouse, J. J. Pekar, . . . Q. Qin (2018). "Accounting for the role of hematocrit in between-subject variations of MRI-derived baseline cerebral hemodynamic parameters and functional BOLD responses." Hum Brain Mapp 39(1): 344-353.

Yeo, B. T., F. M. Krienen, J. Sepulcre, M. R. Sabuncu, D. Lashkari, M. Hollinshead, . . . R. L. Buckner (2011). "The organization of the human cerebral cortex estimated by intrinsic functional connectivity." J Neurophysiol 106(3): 1125-1165.

Zhu, Y. (2004). "Parallel excitation with an array of transmit coils." Magnetic Resonance in Medicine 51(4): 775-784.